Lithofacies and terrestrial sedimentary environments in AMS measurements: a case study from the Neogene of the Oravica River section, Čimhová, Slovakia

Maciej ŁOZIŃSKI[1, *], Piotr ZIÓŁKOWSKI[1] and Anna WYSOCKA[1]

[1] University of Warsaw, Faculty of Geology, Żwirki i Wigury 93, 02-089 Warszawa, Poland

The anisotropy of magnetic susceptibility (AMS) of sedimentary rocks has been used for interpreting a wide range of processes: early rock deformation, palaeotransport directions, as well as the evolution of mineral content. Various sedimentary factors which may determine magnetic susceptibility within lacustrine, river, floodplain and swamp deposits have been examined in the Oravica section of the Orava-Nowy Targ Basin. Multiple components of mineral content: illite, chlorite, smectite, kaolinite and quartz, as well as an unidentified high susceptibility phase make the AMS interpretation of this content ambiguous. However, this method may be useful for tracing early diagenetic geochemical/microbial processes where iron is involved. Some sedimentary processes may be recognized from AMS when an assemblage of parameters is studied together: bulk susceptibility, the degree and shape of anisotropy, principal directions, and the distribution of all these parameters within a set of specimens. Debris-flow processes, as well as lacustrine and floodplain sedimentation are especially well-defined in AMS results. Palaeotransport directions are ambiguous because the rocks have undergone weak deformation that overprints this sedimentary feature. Most specimens represent an oblate shape of anisotropy and show a good correlation of minimum susceptibility axis and normal to bedding plane.

Key words: anisotropy of magnetic susceptibility, facies analysis, terrestrial environments, Neogene, Orava-Nowy Targ Basin.

INTRODUCTION

The idea of using magnetic susceptibility of rocks for geological interpretations was first introduced by Ising (1942) to investigate clay-rich sediment. Ising (1942) noted that magnetic susceptibility of sedimentary rocks is anisotropic with considerably lower (10–20%) susceptibility in the direction normal to bedding. However, the true development of the method application in geology took place after the note of Graham (1954) who indicated the potential of studying this petrofabric feature. Since that time it has been discovered that magnetic susceptibility can record an extensive variety of sedimentary and diagenetic processes as well as tectonic deformation (e.g., Tarling and Hrouda, 1993; Parés, 2015). Since the bulk value of magnetic susceptibility of rock sample is the sum of all minerals' susceptibility of the sample, it is a sensitive tool for tracing variations in mineral composition gained at the deposition time. This can record e.g., quartz/clay minerals ratio, special intercalations like pyroclastic layers, and even a change in clay mineral composition. The latter provides a sensitive tool for analysing climate changes affecting weathering processes and its prod-

uct – clay minerals deposited in a sedimentary basin (Ziółkowski and Hinnov, 2010). The anisotropy of magnetic susceptibility (AMS) is gained at the sedimentation time and is a result of initial orientation of sediment grains having prolate or oblate shapes, and minerals' magnetocrystalline anisotropy. This favours in general oblate character of magnetic anisotropy corresponding to the depositional surface, but can also result in an anisotropy related to sediment transport direction (see summary in Hrouda, 1982). This sedimentary fabric of AMS can be altered afterwards due to reorientation of grains during compaction and tectonic deformation, as well as crystallisation and/or solution of minerals within the rock mass.

It was stated that AMS records even a very slight grade of deformation which usually does not result yet in a presence of macroscopic folds and faults (Parés et al., 1999). This makes the method useful for studying non- and weakly-deformed sedimentary basins, where both sedimentary and tectonic AMS fabric may be observed (e.g., Mazzoli et al., 2012). These features characterize the intramontane Orava-Nowy Targ Basin (Fig. 1), which is expected to offer a good opportunity for AMS investigations.

The wide range of possible sedimentary and tectonic factors affecting AMS fabric can cause uncertainty in interpretation of this kind of studies. The knowledge of possible range of AMS parameters related to lithology and sedimentary processes would be a remarkable improvement in further AMS analysis of the basin, but to achieve this the tectonic factor must be excluded or minimized. For the purposes of this paper, one section of continuous Miocene sedimentary sequence has been

---
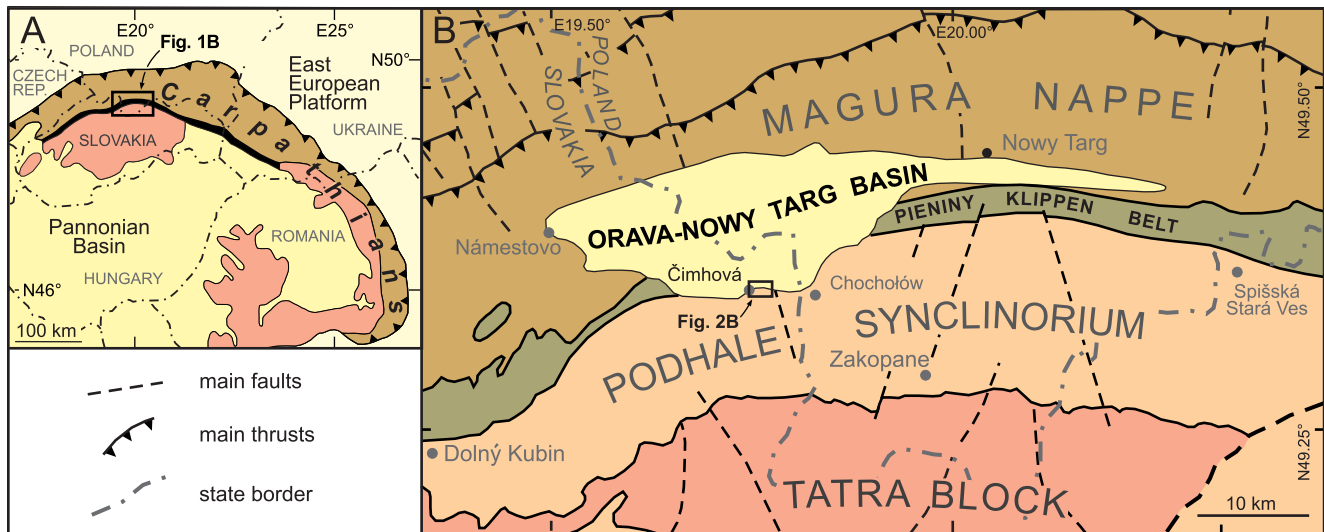
Fig. 1. Schematic map of the northern part of the Central Western Carpathians (A) with the location of the Oravica section near the village of Čimhová (B) (after Lexa et al., 2000; Łoziński et al., 2015, modified)

studied. This allows assuming the same regional tectonic impact for all AMS results within this sequence. The discussed section crops out in the Oravica riverbed near the village of Čimhová (Slovakia). The detailed lithology of rocks and sedimentary environment interpretation can be found in Łoziński et al. (2015), while the discussion on organic-geochemical processes within the former peat and concretionary siderite formation is provided in Bojanowski et al. (2016). This paper introduces an innovative approach of detailed sedimentological analysis compared with a large number of AMS measurements. The aim of this study is to determine the relation between AMS parameters and terrestrial lithofacies characteristics within the well-constrained section of the Oravica River, and to test whether the classical interpretation of tectonic deformation from AMS fabric can be applied to Orava-Nowy Targ Basin deposits.

GEOLOGICAL SETTING

The Orava-Nowy Targ Basin is located at the Polish-Slovakian border within the Western Carpathians (Fig. 1A) and straddles across the Inner/Outer Carpathians border. It was formed in the Middle Miocene within a tectonic depression during the Carpathian strike-slip movements along SW–NE or W–E trending fault zones (Baumgart-Kotarba, 1996, 2001; Nagy et al., 1996; Pomianowski, 2003; Struska, 2008; Tokarski et al., 2012). The basin infill is composed mainly of claystones, clayey siltstones, sandstones and conglomerates with intercalations of lignite, pyroclastics, and freshwater limestones (Sikora and Wieser 1974; Watycha, 1976; Kołcon and Wagner, 1991; Jaroszewicz et al., 2013; Łoziński et al., 2015) deposited in river, alluvial fan, lake, and swamp settings. Detrital material is represented mainly by quartz, organic matter and clay minerals: beidellite, chlorite and illite (Wiewióra and Wyrwicki, 1980). A clastic sedimentary sequence of the basin infill, up to 1.3 km thick, originated presumably from older structural units exposed in the basin vicinity: the Magura Nappe, Pieniny Klippen Belt

and Podhale Synclinorium (Fig. 1B). They are of Jurassic–Early Miocene age and represent sedimentary sequences generally composed of marine limestones, sandstones, and mudstones. The southern part of the basin in the study area is underlain by the Podhale Synclinorium being part of the Central Carpathian Paleogene Basin. It is composed of the Lutetian–Bartonian to Egerian sandstones, mudstones, calcareous claystones and rare conglomerates deposited mainly from turbidity currents (Gross et al., 1993; Olszewska and Wieczorek, 1998; Soták, 1998a, b; Garecka, 2005). Marginal parts of the Orava-Nowy Targ Basin underwent uplifting probably in the Pleistocene (Tokarski et al., 2012) resulting in tilting up to 25° and erosion.

The outcrop is located near the southern margin of the basin along the Oravica River banks (Fig. 2). Łoziński et al. (2015) have described an over 80 m sedimentary sequence deposited in lake, river, floodplain and swamp environments. Several lithofacies from the lower and middle parts of the sequence have been subjected to a detailed study (Fig. 2). The sedimentation began with the matrix-supported disorganized monomict breccia (Gmm) consisting of muddy matrix with heavily weathered sandstone and mudstone clasts from the underlying Podhale Synclinorium. This is followed by the lacustrine sedimentary sequence: from claystones (CL) and laminated siltstones and claystones (Fl) deposited from suspension, to heterolithic silty (Hf) and sandy (Hs) deposits of low-density turbidity currents. These are overlain by a terrestrial sequence deposited generally in a river setting: massive siltstones (Fm) with local occurrences of siderite and rhodochrosite concretions (Bojanowski et al., 2016) deposited on floodplains, and trough (St) and planar cross-bedded sandstones deposited in fluvial channels. This is followed by an alternation of river, floodplain, and swamp sequences represented by cross-bedded sandstones, massive siltstones (Fm), coals (C), coaly claystones extremely rich in plant detritus (CCL), and pure claystones accompanying coals and coaly claystones deposited probably in small ephemeral lakes (named here CL2 to distinguish from offshore lacustrine clays CL and CL_1). Two lithofacies occur as unique intercalations: the tuffite layer (T) and the freshwater limestone layer (L).
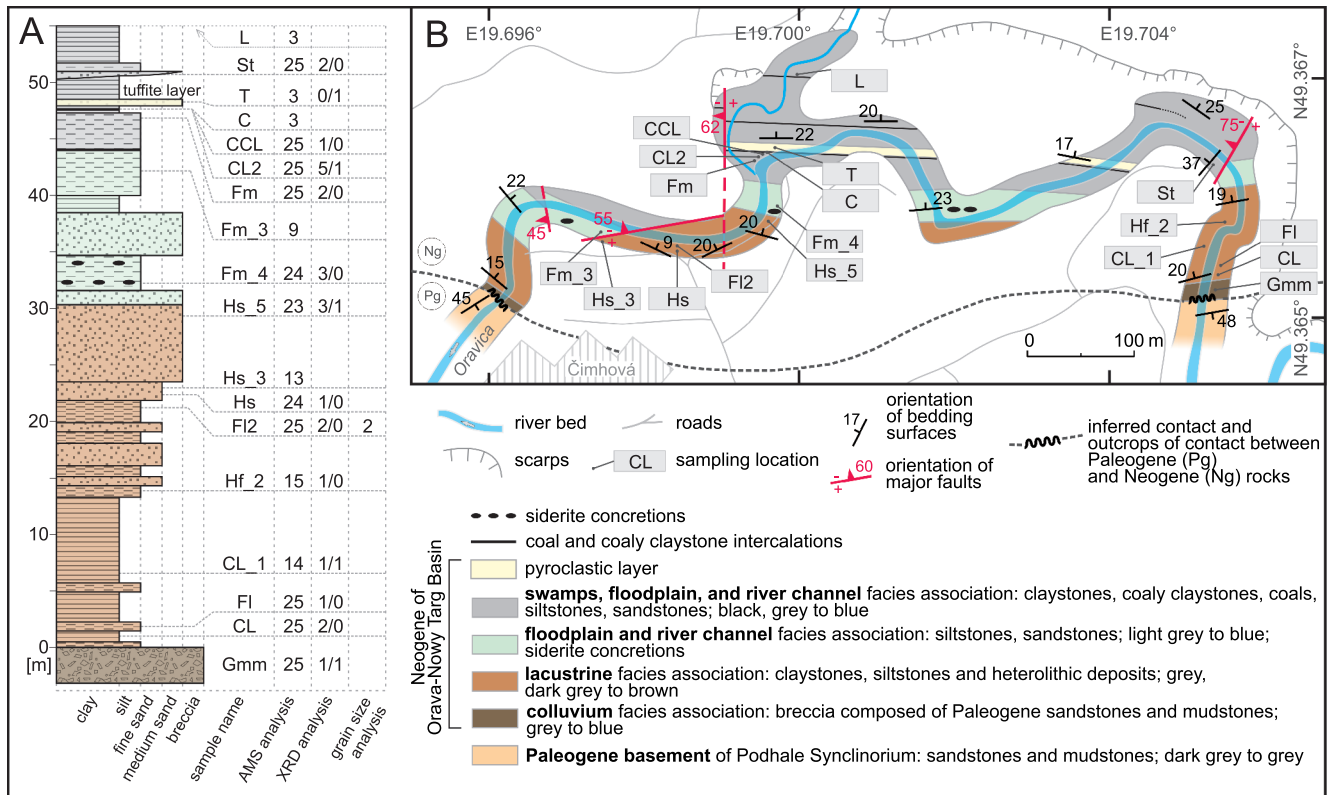
Fig. 2A – lower part of the Oravica section sedimentary log (after Łoziński et al., 2015), sampling position and numbers of analysis: anisotropy of magnetic susceptibility (AMS), X-ray diffraction (XRD) with numbers of powder/oriented analysis, and laser diffraction grain-size analysis; B – schematic geological map showing groups of lithofacies (after **Łoziński et al., 2015; Bojanowski et al., 2016,** modified) according to the sedimentary environment; sampling locations are marked with grey boxes

METHODS

The study was conducted on cylinder-shaped specimens (n = 322, diameter 25.4 mm, and length 22 mm) collected using 15 cm long brass samplers (Fig. 3) hammered with a rubber hammer into deposit exposed in the field. The material col-
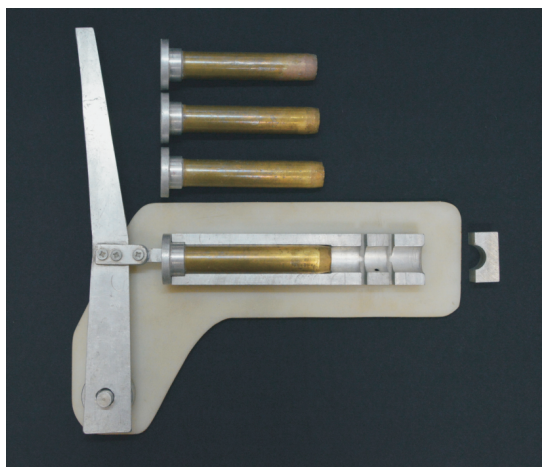
Fig. 3. AMS sampling equipment

Brass 15 cm long samplers which are hammered into sediment, and an aluminum tool for pushing out and cutting acquired material into $\varnothing$ = 25.4 x 22 mm cylinder AMS specimens

lected with the sampler was pushed out with a special tool (Fig. 3), and then cut into 22 mm long specimens (from 1 to 3 specimens). Sampler position was horizontal and sampler azimuth was measured during sampling in the field. The statistical approach was intended to give the picture of magnetic susceptibility parameters on the two analytical levels: within a group of specimens collected from one lithofacies, and between groups of specimens collected from different lithofacies and from different areas of the outcrop. To achieve this, 15 spots representing different lithofacies were selected within the outcrop. Within each lithofacies a set of specimens has been collected with the same azimuth. A set of specimens (up to 25) collected from one lithofacies and within 0.5 m of outcrop will be referred to as a "sample" in this article. A sample name is a lithofacies abbreviation and, sometimes, a sample number (e.g., 3 samples of massive siltstone are: Fm, Fm_3, and Fm_4; Fig. 2). Specimens were measured at field intensity 2 ÷ 200 A/m and frequency 976 Hz using a *MFK1-FA* kappabridge with a spinning holder (AGICO, Czech Republic), at the Institute of Geophysics, Polish Academy of Sciences. The coal (C), tuffite (T), and limestone (L) lithofacies represent lithified rocks, what excluded the possibility of using a hammered sampler. Instead, the bulk susceptibility of non-oriented specimens was measured with a portable MS3 magnetic susceptibility meter equipped with a MS2E sensor (Bartington Instruments, UK) at the European Centre for Geological Education in Chęciny.

All magnetic susceptibility parameters discussed here [mean magnetic susceptibility (Km), anisotropy degree (P), anisotropy shape (T), lineation (L), foliation (F), and ellipsoid orientation] are determined by a magnetic susceptibility tensor of rank two (Jelínek, 1977). This tensor can be represented as a symmetric

matrix 3 x 3, which has been obtained for each specimen from a *MFK1-FA* kappabridge, and transformed between geographic, specimen, and bedding coordinate systems. Most convenient for the analysis are three principal susceptibilities $k1 \geq k2 \geq k3$ and their corresponding directions of axes in space. The mean susceptibility value $Km = (k1 + k2 + k3)/3$ is an important indicator for the mineral content of specimen.

The acquired data has been processed using the *Anisoft 4.2* software (Chadima and Jelínek, 2009), and the R language and environment for statistical computing (R Core Team, 2015) with the *ggplot2* module (Wickham, 2009) and the RStudio integrated environment (RStudio Team, 2015).

The mineral composition was examined with X-ray diffractometry (XRD) using a *X'Pert PRO MPD* instrument equipped with a cobalt lamp (PANalytical B.V., the Netherlands) at the Institute of Geochemistry, Mineralogy and Petrology, Faculty of Geology, University of Warsaw. The Bragg-Brentano geometry was used with 2θ angle recorded within the range of $3.7 \div 78.0°$ and the accuracy of $0.026°$. The 25 powder samples (mass 4 g, record time 3 h) were obtained from AMS specimens (mass 20 g) to define the relation between mineral composition and magnetic susceptibility. The five samples were chosen for additional clay mineral analysis. They were crushed and spread in deionised water with admixture of sodium pyrophosphate to prevent coagulation. After 24 hour sedimentation the remaining suspension was dried on glass plates and recorded with an X-ray instrument (record time 1 h): pure, ethylene glycol saturated, and heated in 500°C for 3 h.

The laser diffraction analysis of grain size was performed on two mechanically powdered and water-dispersed specimens after 4 minutes of ultrasonic treatment, using a *Mastersizer 3000* instrument (Malvern Instruments Ltd, UK) at the Institute of Ceramics and Building Materials in Warsaw.

RESULTS

MAGNETIC SUSCEPTIBILITY AND ITS MINERALOGICAL CARRIERS

The bulk volume magnetic susceptibility measured on 322 specimens has revealed a wide variety of mean susceptibility values (Km) ranging from 85 to 5560 x 10^{-6} [SI]. The 50% of specimens falling in a range between 25 and 75% quantiles have susceptibility values from 160 to 300 x 10^{-6} [SI] (Fig. 4, see "all"), which is a relatively narrow range compared to all obtained values. Value 300 x 10^{-6} [SI] is also a good limit for consideration because 11 out of 15 samples have their median value below this level (except for Fl, St, Fm and CL2), and many samples have all their specimens be-

low this level. The basic content for all investigated specimens: quartz, illite, kaolinite, smectite, chlorite and calcite revealed in XRD analysis can easily explain the obtained range of mean susceptibility mentioned above (Km <300 x 10^{-6} [SI]) in a simple mineral effect summation model (Table 1). This means that a large number of specimens has similar mineral content without admixtures of mineral grains with strong susceptibility (mainly ferromagnetic grains). Components constituting the susceptibility
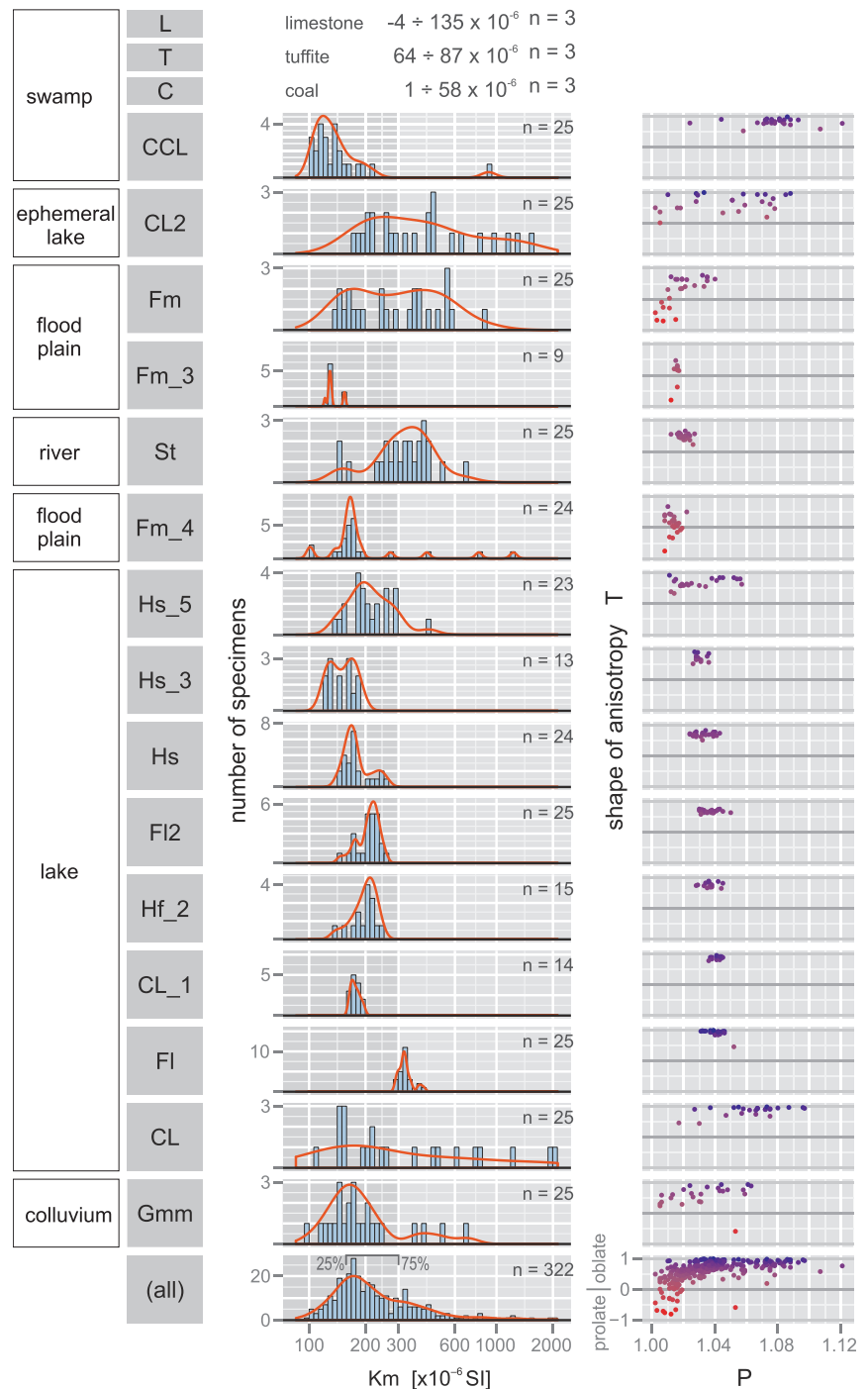
Fig. 4. Mean susceptibility (Km), degree of anisotropy (P), and shape of anisotropy (T) distribution within samples and within the entire population of AMS specimens

Quantiles 25 and 75% are shown in the plot of all specimens; number of specimens within a sample is denoted by n; samples are collated with interpreted sedimentary environments (Łoziński et al., 2015); the bulk susceptibility of coal (C), tuffite (T), and freshwater limestone (L) specimens have been measured with a portable susceptibility meter

value within the discussed group of specimens are represented by a mixture of clay minerals, mainly chlorite and illite, which are widespread in all analysed lithofacies. The comparison of Km values and sedimentary environments reveals that lake lithofacies represent samples with dense Km distribution around their median with relatively small Km values (<300 x 10⁻⁶ [SI], except for CL, Fl, and Hs_5 – initial and final lake lithofacies), while other lithofacies have various Km distributions (Fig. 4).

The most common mineral of which higher content may result in lower magnetic susceptibility is quartz (Table 1A). Other minerals with low or negative susceptibility, i.e. kaolinite, calcite,

and dolomite, are considered to have too small contents (<5%) to have a noticeably decreasing impact on the mean susceptibility. A higher quartz content relation to lower magnetic susceptibility was positively examined in two varied specimens from one coherent sample Fl2 in XRD analysis (Fig. 5). Also, a grain-size measurement was carried on these two samples, showing that the lower susceptibility sample with higher quartz content is enriched in 12–130 μm sizes (10% volume), while 0.5–72 μm sizes are common for both specimens (Fig. 6). These facts show that the sedimentation of lacustrine clayey siltstones may have been slightly altered in terms of grains size and quartz content, resulting in susceptibility variation within the range of 160–246 x 10⁻⁶ [SI] (values for two discussed specimens).

Low susceptibility values can also be a result of noticeable organic matter admixture, which can be observed in lithofacies CCL (Km within the range of 104–218 x 10⁻⁶ [SI], compare with low coal susceptibility in Fig. 4 and Table 1). The presence of indeterminable organic matter can be macroscopically inferred from specimen colour ranging from dark grey to black. The susceptibility of tuffite specimens falls within the range of 64–87 x 10⁻⁶ [SI], and, according to XRD analysis, it reflects its dominating smectite content. Although the tuffite is a unique layer within the Oravica section, the smectite occurrence within other lithofacies, resulting from volcanic eruptions or pyroclastics redeposition, is possible. Additionally, small values of susceptibility of freshwater limestone, falling within the wide range of –4–135 x 10⁻⁶ [SI], have been recorded within the upper part of the Oravica section.

Only 25% of specimens fall within the wide susceptibility range of 300–5560 x 10⁻⁶ [SI] and have generally sparse distribution (Fig. 4). This can be easily traced with the interquartile range value (IQR = quantile 75% – quantile 25%) calculated for every sample. The sparse distribution is represented by samples: Gmm, CL, Hs_5, Fm_4, St, Fm, and CL2 which have large IQR values within the range of 68–447 x 10⁻⁶ [SI]. The dense distribution is represented by samples: Fl, CL_1, Fl2, Hf_2, Hs, Hs_3, Fm_3, and CCL having IQR 3–38 x 10⁻⁶ [SI]. All samples showing high Km values have a high IQR value, except for unusual sample Fl. This sample has dense distribution (IQR = 24 x 10⁻⁶ [SI]) while having larger Km values: 290–410 x 10⁻⁶ [SI], probably due to the high clay mineral content.

T a b l e   1

Approximate values of bulk magnetic susceptibility

A Magnetic susceptibility of rock components	
Mineral/rock	bulk susceptibility [x10⁻⁶ SI]
Quartz	−13 ÷ −17 [1]
Illite	410 [1]
Muscovite	65 ÷ 402 (mean 110) [2]
Montmorillonite	330 ÷ 350 [1]; 44 ÷ 103 [3]
Beidellite	86 ÷ 116 [3]
Chlorite	210 ÷ 1390 (mean 490) [2]
Kaolinite	−50
Calcite	−7.5 ÷ −39 [1]
Siderite	1300 ÷ 11000 [1]
Gypsum	−13 ÷ −29 [1]
Pyrite	35 ÷ 5000 [1]
Coal (rock)	25 [1]
B Magnetic susceptibility of compounds (models)	
5 – Q, 35 – illite, 35 – smectite, 20 – chlorite, 5 – kaolinite; [in %]	0.05* (−15) + 0.35*400 + 0.35*100 + + 0.20*1400 + 0.05* (−50) = 452
55 – Q, 20 – illite, 20 – smectite, 5 – chlorite; [in %]	0.55* (−15) + 0.20*400 + 0.20*100 + + 0.05*1400 = 162

A – bulk magnetic susceptibility values for minerals occurring in the study area (excluding magnetic minerals); 1 – Hunt et al. (1995) and references therein, 2 – Martín-Hernández and Hirt (2003), 3 – Callaway and McAtee (1985) – 2.35 g/cm³ for montmorillonite and 2.15 g/cm³ for beidellite densities are assumed for calculation from mass susceptibility; **B** – magnetic susceptibility of quartz and clay mineral compounds show a possible susceptibility range matching measured values
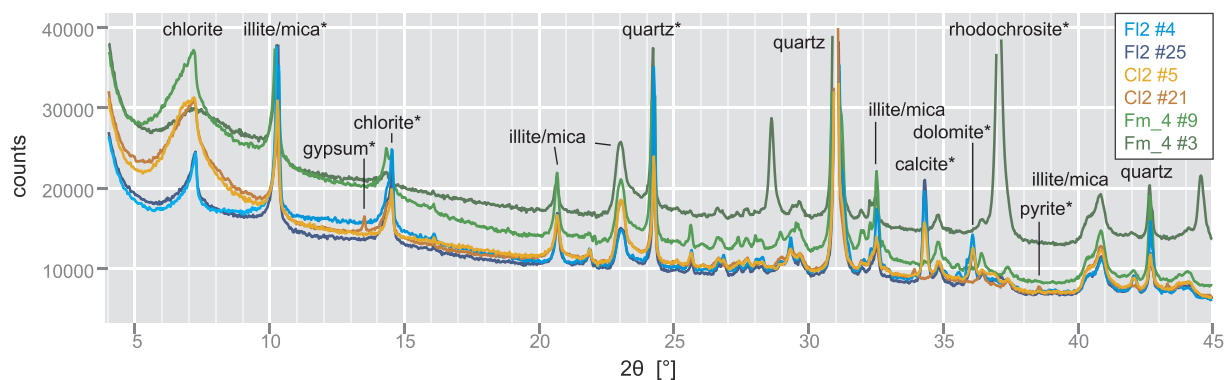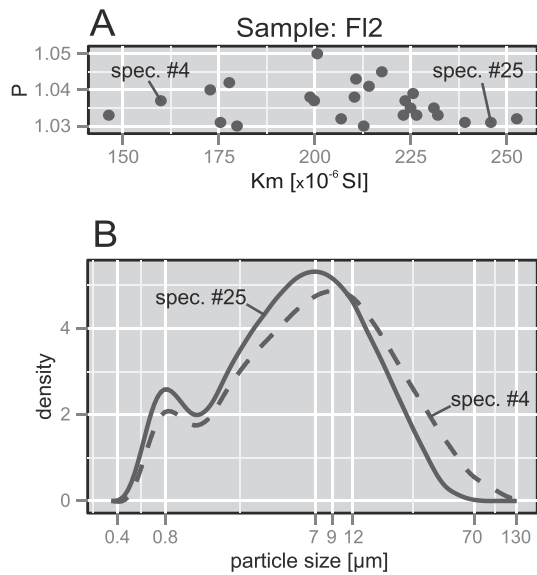

Fig. 5. X-ray traces for six powder specimens (pairs from three lithofacies) with main reflections identified

Reflection intensities used in a quantitative comparison are marked with (*); various ratios of chlorites to smectites can be seen at 2θ around 7° as a differentiated chlorite peak shape; a higher background of Fm_4 #3 specimen is a result of Mn in rhodochrosite

Fig. 6A – specimen population of sample Fl2 in the plot of anisotropy degree (P) vs. mean magnetic susceptibility (Km) with two investigated specimens #4 and #25; B – grain-size analysis of those two specimens showing coarser grain sizes within lower susceptibility specimen #4

High Km values (Km > 300 x 10^{-6} [SI]) cannot be explained by the model introduced before (Table 1B). Chlorite, being the only examined mineral which has considerably high magnetic susceptibility, has not been found in XRD analysis in necessary quantities to support this model. As an example, two specimens Cl2#5 and Cl2#21 with susceptibilities of 178 and 1543 x 10^{-6}[SI], respectively, have been compared in terms of XRD trace but show no significant difference (Fig. 5). The component responsible for high Km values must be either a non-crystalline phase or ferromagnetic grains with strong magnetic susceptibility but very low content undetectable in XRD. The sparse distribution of high Km values within the corresponding lithofacies suggests that this component has highly random content (Fig. 4). It occurs generally in terrestrial settings and exceptionally in initial lacustrine lithofacies CL, which is more like lithofacies CL2 than other lacustrine lithofacies. It is possible that the strong susceptibility component is a detrital component (e.g., heavy minerals), which has been separated from clays and quartz during transport and has not reached a lake setting. It might have also been a result of some early diagenetic geochemical/microbial processes that occurred only in a terrestrial setting. Considering the fact that high Km values are common in claystone lithofacies CL and CL2, the latter hypothesis is more probable. The explanation of the nature of this component requires additional detailed analysis, which is beyond the scope of this paper.

ANISOTROPY OF MAGNETIC SUSCEPTIBILITY

Comparison of the principal susceptibilities k1, k2, and k3 leads to defining useful anisotropy parameters: degree of anisotropy P = k1/k3, lineation L = k1/k2, foliation F = k2/k3, and shape of anisotropy T = [2log(k2)–log(k1)–log(k3))/(log(k1)–log(k3)] (Hrouda, 1982 and references therein). The parameter T >0 denotes oblate shape, while T <0 denotes prolate shape. The plot of T–P is shown in Figure 4. Lacustrine samples (except for CL and Hs_5) represent a narrow range and medium values of ani-

sotropy P (1.025–1.050) confirming that lacustrine lithofacies are coherent from magnetic susceptibility perspective. Increasing content of thicker grains within lacustrine samples Hs, Hs_3, and Hs_5 causes a slight decrease of anisotropy P. The most incoherent sample is Hs_5 which is a heterolithic deposit composed of sandstones to claystones. Samples Hs and Hs_3 represent a deeper and less varied lake environment. Samples CL and CL2 have a similar wide range of anisotropy P, which may be caused by an unknown strong magnetic component as well as intercalations of lithofacies Fm. Sample CCL, rich in organic matter, has the largest degree of anisotropy P (mean P = 1.077, maximum P = 1.121) among all samples, and very oblate anisotropy shape T. It seems that a compound of clay minerals and organic matter (probably plant detritus) is the most anisotropic lithology, although pure coals are known to have very weak anisotropy (Hrouda, 1982). Floodplain lithofacies represented by samples Fm, Fm_3, and Fm_4 have medium to very low anisotropies and different shapes of anisotropy T (from –0.80 to +0.77). This very unique feature has been observed only within lithofacies Fm, where 22 ÷ 28% of specimens have prolate shape (T <0). Lithofacies Fm, being clayey siltstone, has been distinguished from others on the basis of generally massive structure with very rare poorly preserved lamination and typical bluish-grey colour (Łoziński et al., 2015). Its massive structure is interpreted as a result of either undifferentiated detrital components or bioturbation. The latter may be related with a destructive role of small plant roots. Although plant remnants are generally not retained within lithofacies Fm, the root traces have been preserved within siderite concretions (Bojanowski et al., 2016). The bioturbation might have lead to differentiation and general reduction of depositional anisotropy. Also, deposits of floodplain may have contained a considerable amount of anisotropic muddy clasts deposited chaotically during fast flood sedimentation. This irregular fabric of weak anisotropy might have been overprinted by tectonic lineation, which, if greater than foliation (L > F), can result in a negative shape parameter (T <0). Fluvial channel lithofacies St, having coarser grains with higher quartz content than lithofacies Fm, has a low but coherent degree of anisotropy and oblate shape of anisotropy. This rock is cohesive due to some clay mineral content which probably causes noticeable anisotropy. Considering the remarkable current strength in rivers with trough cross-bedding, clay minerals might have been transported as silt- and sand-sized intraclasts or lithoclasts. Sample Gmm has a wide variety of anisotropy P values (from 1.005 to 1.063) and shape parameter T (0.236 to 0.927), and is similar to heterolithic sample Hf_5. This is because both of them are heterogeneous samples consisting of clayey to sandy grains.

Since the high susceptibility (Km > 300 x 10^{-6} [SI]) is generally dominated by an additional (unknown) component in rock mineral composition, it should reveal its own anisotropy in the anisotropy (P) to susceptibility (Km) plot (Fig. 7). According to the plot with all specimens, excluding sample Fl (Fig. 7A), three arbitrary groups of specimens have been introduced. Group 1 represents specimens with low susceptibility (Km < approx. 250 x 10^{-6} [SI]) and dense Km distribution within the sample. Groups 2 and 3 represent specimens with high susceptibility and sparse Km distribution. Groups 2 and 3 differ in respect of the degree of anisotropy (P), suggesting two different mechanisms or mineral components responsible for high susceptibilities. Group 2, having high P values, appears only within lithofacies Gmm, CL, and CL2 (Fig. 7B), while group 3, having low P, appears mainly within lithofacies Fm, Fm_4, and St (Fig. 7C). Both groups seem to have a downward trend. This suggests that the strong Km component has rather low anisotropy and its raising content decreases P value inherited from the
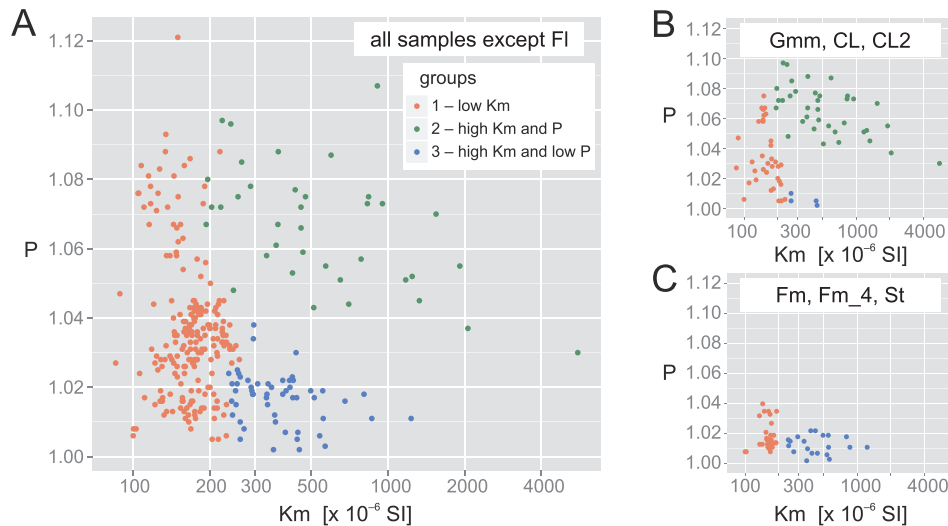
Fig. 7A – plot of anisotropy degree (P) vs. mean susceptibility (Km); specimens with Km > 250 x 10⁻⁶ [SI] fall into two separate groups; B – plot for samples constituting group 2; C – plot for samples constituting group 3; note a downward trend within both groups 2 and 3, suggesting that the high susceptibility component has a lower anisotropy degree than the clay-quartz matrix

anisotropic compound of clay minerals and quartz. If the strong susceptibility component is a kind of early diagenetic phase it might have gathered around detrital grains causing anisotropy imitating grain shapes. This possibility might have led to high anisotropy within group 2 (Fig. 7B) due to higher content of platy clay minerals, and to low anisotropy within group 3 (Fig. 7C) with higher content of isometric quartz grains.

X-RAY DIFFRACTION

Twenty-five specimens with various magnetic susceptibility and degree of anisotropy have been investigated in powder X-ray diffraction in order to find a correlation between magnetic properties and mineral composition. It has been found that all specimens contain the following minerals in major quantities: quartz, smectite, chlorite, and illite/mica (Fig. 5). Kaolinite as well as mixed-layer clay minerals were found in minor quantities in a detailed clay minerals study. The specimens contain also minor quantities of calcite, dolomite and plagioclase (<5%). Six specimens contain pyrite and five specimens contain gypsum in trace amounts. However, these two minerals show high concentrations in coaly claystone (CCL) lithofacies abundant in organic matter. In four specimens, rhodochrosite was found. No noticeable siderite amount was recorded, but Fe in dolomite or rhodochrosite structure is possible.

This compound of minerals has a large number of parameters which can be involved in determining magnetic susceptibility: contents of at least four main components, as well as smectites and chlorites type, especially amount of Fe in the chlorite structure. This makes detailed recognition of clay minerals, quantification and susceptibility modelling very complex. Therefore a simplified approach has been used for the purpose of this paper, based on the idea introduced by Chung (1974a, b). The method involves comparing reflection intensity of minerals within a specimen without internal standard and reference intensity. Every intensity value for mineral peak i is equal:

$$I_i = X_i \cdot K_i \cdot A$$

where: I – peak intensity, X – volume of mineral causing reflection, K – constant parameter dependent on the instrument and mineral characteristics, and A – mass absorption being a function of all minerals in sample.

The parameter A is unknown and constant but different for every measured sample. However, when comparing intensities of chosen reflection of two minerals in a single sample, parameter A is not needed:

$$\frac{I_i}{I_j} = \frac{X_i \cdot K_i \cdot A}{X_j \cdot K_j \cdot A} = m \cdot \frac{X_i}{X_j}$$

where: $m = K_i/K_j$ is unknown but constant for minerals i and j thorough all samples; I_i/I_j is not exactly the ratio of mineral contents X_i/X_j, but is always proportional to it and this proportion can be compared across samples and serve as a parameter for correlations with magnetism.

Several 2θ angles have been chosen to determine intensities for quartz, chlorite, illite/mica as well as for calcite, dolomite, rhodochrosite, gypsum and pyrite (Fig. 5, see reflections with an asterisk). Illite and mica reflections overlap, so they will be considered here together and referred to as illite. Smectites do not show any usable reflection, but appear as an alteration of XRD trace at low 2θ angles which can be seen: between Fl2 and Cl2 lithofacies (4–10°), between specimens #5 and #21 of lithofacies Cl2 (7°), and between specimens #9 and #3 of lithofacies Fm_4 (4–10°). Smectites were though neglected in this analysis. The intensity values have been measured from the reflection top to the level of trace background, which was linearly interpolated under reflection.

The basic ratios studied here are: illite to quartz (ill/Q), and chlorite to quartz (chl/Q), which were used to construct Figure 8. Additionally, the proportion of (ill/Q) to (chl/Q) equals:

$$\frac{ill\,/\,Q}{chl\,/\,Q} = \frac{ill}{chl} = \tan(\alpha)$$

so the illite to chlorite ratio can be also obtained from this plot from the tangent of angle between specimen point-origin line and horizontal axis.

The (ill/Q) and (chl/Q) ratios revealed good linear correlation (Fig. 8; Pearson coefficient corr = 0.89), which means that the ill/chl ratio is similar for all specimens, while the quartz to clay minerals ratio varies (however, smectite content is not known and probably not constant). The exception is lithofacies Fm_4, where all three specimens have lower chlorite content – this fact will be discussed hereafter.
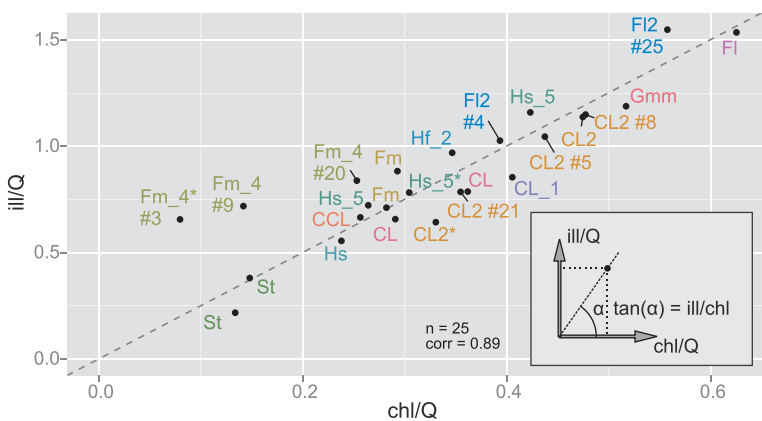
The above observation has sedimentological implication – chlorite and illite have been probably transported and deposited together, but separately from quartz. Moreover, various sedimentary environments – from distal offshore lake through river channel and floodplain to swamp lithofacies – have had the same source for chlorite and illite. Lithofacies Gmm, which was interpreted as debris-flow sediment containing eroded and disintegrated rocks of older underlying unit – mudstones and sandstones of the Podhale Synclinorium (Łoziński et al., 2015), also fits the discussed illite/chlorite ratio. This supports a hypothesis that the Podhale Synclinorium was the main source of clastic material for the Orava-Nowy Targ Basin infill in the study area. The variable ratio of clays to quartz might have been the result of transportation as grains of different sizes. This was positively verified in grain-size analysis (Fig. 6) of two specimens #4 and #25 from the offshore lake lithofacies Fl2 with different chlorite/quartz and illite/quartz ratios (Fig. 8), as mentioned before.

The most unusual ill/chl ratio has been recorded in specimen Fm_4#3. This specimen contains also an unusual concentration of rhodochrosite which was found in smaller quantities in three other specimens (Fig. 8, see asterisk). This mineral, which occurs in specimens with high Km values (200–800 x 10^{-6}), has been also noted in lithofacies Fm_4 by Bojanowski et al. (2016). It has been found that rhodochrosite had cemented rhizoliths and occurred in siderite-bearing horizons which originated in an anoxic zone with bacterial methanogenesis below an active peat. Specimen Fm_4#3, collected from a siderite-bearing horizon (but not a concretion), has revealed rhodochrosite but no siderite. It contains also relatively much smectite (Fig. 5). Other specimens Fm_4#9 and Fm_4#20 collected up to 2 m above Fm_4#3 also have a high illite/chlorite ratio (Fig. 8). This suggests that the whole sediment in this area might have undergone geochemical and/or microbial processes related to further rhodochrosite and siderite precipitation and alteration of clay minerals. It is also likely that these processes might have been responsible for the origin of minerals or amorphous phase in rhodochrosite-bearing specimens. However, high Km values cannot be treated as an indicator for rhodochrosite occurrence which is rare.

As shown above, chlorite and illite can be considered as one component with an approximately constant chlorite-illite ratio. They also have the highest magnetic susceptibility among minerals recorded in the XRD study (Table 1A). Thus, the chlorite-quartz or illite-quartz ratio is expected to have a positive correlation with magnetic susceptibility (Fig. 9A). This should be true for specimens which do not have susceptibility determined by strong ferromagnetic grains, so the comparison was restricted to specimens with Km < 350 x 10^{-6} [SI]. The chlorite-quartz towards Km plot shows weak positive correlation (corr = 0.59), however, it is insufficient for ill/chl ratio calculation from Km. The chl/Q variation at the same Km value may be very high – specimen Gmm has above 3 times higher chl/Q than specimen St at Km = 160 x 10^{-6} [SI]. This suggests that some other unknown factor is involved and bulk mean susceptibility Km cannot be used to compare the content of two different lithofacies. Trends within coherent samples Fm_4, Fl2, and Cl2 (Fig. 9A, colour dotted lines) are upward as expected, while incoherent heterolithic sample Hs_5 contains two specimens with a downward trend. Perhaps, this method could be useful within one coherent lithofacies.

The chl/Q relation to the degree of anisotropy is expected to show some correlation because clays have magnetocrystalline anisotropy while quartz is isotropic. This correlation is surprisingly very poor (Fig. 9B; corr = 0.25), which means that the degree of anisotropy parameter cannot be used as an indicator for the chl/Q ratio. And, likewise the chl/Q to Km relation, some other factor must be responsible for this observation.

DIRECTIONS OF AMS ELLIPSOID

The great advantage of the AMS method is the possibility to obtain a three-dimensional picture of magnetic anisotropy which can be afterwards applied to geological interpretation. There are several geological processes which can be involved in altering the AMS pattern. Susceptibility symmetrical about vertical axis k3 (perpendicular to bedding) is gained at the deposition time, with principal susceptibility k1 approximately equal to k2 and axes directed randomly. This can be slightly modified if the deposition undergoes in a current resulting in elongated sediment grains lying parallel to the current direction (Hrouda, 1982 and references therein) or perpendicular, if grains are rolling (Tarling and Hrouda, 1993). This results in separation of k1 from k2, with k1 oriented along the current direction or along the rolling axis, depending on the transport regime. The same effect of separation can be also obtained if a tectonic stress field is applied. It was

Fig. 8. Plot showing the relative volume ratios of: chlorite to quartz (horizontal axis), illlite + mica to quartz (vertical axis), and illite + mica to chlorite (tangent α) based on the comparison of chosen XRD reflection intensities

Dashed line shows linear approximation of data; specimens containing rhodochrosite are marked with (*); specimens show a good correlation (Pearson coefficient – corr) between illite + mica and chlorite content, except for lithofacies Fm_4; note that the ill/Q and chl/Q ratios are proportional but not equal to the actual volume ratios for these minerals; for other explanations see text and Figure 5

Fig. 9A – relation of the chlorite to quartz ratio (chl/Q) to mean magnetic susceptibility (Km); B – relation of chlorite to quartz ratio (chl/Q) to anisotropy degree (P)

Trends within lithofacies (colour dotted lines) are variable, although the general trend (black dotted lines) is upward; the weak correlation (corr) in both plots shows that Km and P parameters cannot be used directly as an indicator for the chl/Q ratio; specimens presented here are restricted to Km < 350 x 10^{-6} [SI] in both plots

observed (Winkler et al., 1997; Parés et al., 1999) that k1 axis rotates towards the smallest compression direction, while k3 towards the largest. Therefore, burial compaction, which can be treated as vertical deformation, generally strengthens the original sedimentary AMS pattern (Parés, 2015). If the deformation is raising, axes k3 rotate towards the strongest deformation direction, going through an intermediate AMS pattern when axes k2 and k3 are mixed along a common circle. This relation of the AMS characteristics to sedimentary and tectonic processes brings a question what interpretation can be achieved from AMS directions in our study area.

A plot of all measured specimens and the mean susceptibility directions (Fig. 10A; statistics of Jelínek, 1978) reveals a sedimentary pattern with k1 and k2 distinguishable but not apparently separated from each other. This points to the "earliest deformation stage" according to Parés et al. (1999). Rocks are generally tilted ca. 10–25° to the north, as is clearly visible from k3 axis tilted 14° from vertical direction.

Since the sampling method involves some compression impact on specimen towards the sampling direction, it can overprint the anisotropy fabric of geological origin. This should be traceable in a specimen coordinate system projection as k1 directions preferably lying perpendicularly to sampling direction (projection north), assuming that different sampling azimuths have been applied. However, this effect has not been observed within the group of studied specimens (Fig. 10B). Assuming that separation of k1 from k2 is of tectonic origin, N–S contraction or W–E extension might have occurred. Axes grouping seems to comply with bedding dip direction with k1 lying normally (Fig. 10C).

This general view becomes more complex in details because lithofacies vary from each other. The most unusual lithofacies is Gmm, which was the only one that revealed chaotic distribution of susceptibility axes directions (Fig. 11A). This pattern does not fit any of the AMS patterns discussed above, because none of the principal susceptibility axis within Gmm is grouped around its mean direction. This lithofacies is a breccia consisting of heavily weathered sandstones and mudstones (Łoziński et al., 2015). The matrix contains probably the same silty and clayey components as clasts but disintegrated. This sediment was interpreted as a result of "cohesive, clay-rich debris flow" which was probably moving on a slope. The AMS results of specimens collected from the breccia matrix confirm

this interpretation very well, revealing a chaotic structure of disintegrated, moved and rotated rock mass. They deny also a river setting origin, where a clast-supported structure would be made first. Free spaces in between would be filled afterwards with horizontally laminated deposits, but in this case the AMS results show no consistent bedding. Scattered k3 directions show some tendency to be tilted southward. This can be speculatively attributed to a southward palaeoslope inclination supporting the interpretation of palaeorelief gradient conclusions inferred from transport directions (Łoziński et al., 2015). Anyway, the AMS method seems to be very useful for recognizing and analysing debris-flow deposits, especially if heavily disintegrated clasts cannot be observed macroscopically.

Lithofacies Gmm is directly overlain by lithofacies CL – the sedimentary contact is confirmed by topmost breccia clasts being surrounded by laminated deposits. Lithofacies CL has the sedimentary AMS pattern with axes k1 and k2 distributed sparsely in the bedding plane with weak separation of those two axes (Fig. 11B). This pattern is also present within all clay-rich lithofacies: FI, CL_1, CL2, and CCL, while other silt- and fine sand-rich lithofacies have axes k1 and k2 grouped around their means (Fig. 11C). It is important to note that k1 and k2 directions distribution should not be treated as the unequivocal deformation indicator because it seems to be clay-content dependent. It may also happen that many lithofacies with coherent k1 and k2 directions presented together in a single plot result in incoherent k1 and k2 directions of the total set, because the mean directions of axes k1 and k2 differ between lithofacies. In this sense, the AMS pattern type may turn out to be dependent on the number of specimens.

A high value of bulk magnetic susceptibility implies the presence of an additional mineral phase having strong susceptibility. This phase (sometimes individual grains) may alter the magnetic pattern in a random manner. This is shown in Figure 11 where direction axes have been shown depending on the susceptibility magnitude (if Km >300 x 10^{-6} [SI] then the symbol is unfilled). Most of high-susceptibility specimens are close to mean directions, but a few specimens represent random directions (Fig. 11C). The latter may worsen the precision of analysis, however, this issue has been neglected in this paper due to low number (2%) of such "unfitted" specimens.

With a very weak tectonic alteration, the AMS pattern reveals the main sedimentary feature – axis k3 being perpendicu-
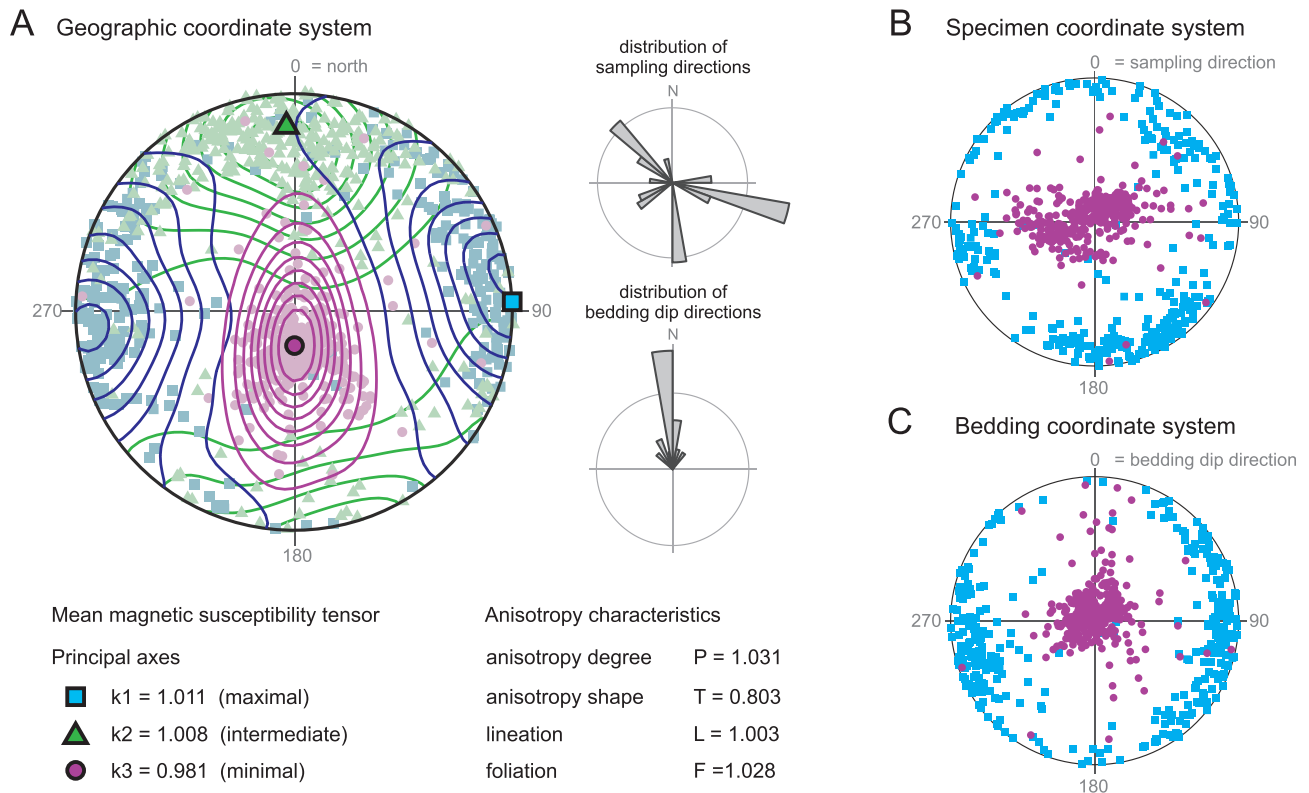
Fig. 10. Distribution of k1 (blue), k2 (green, only A), and k3 (violet) axes directions of the mean magnetic susceptibility tensor for all 322 specimens (lower hemisphere equal-area projection), and distributions of sampling and bedding dip directions (grey bars)

A – distribution in geographic coordinate system; contour lines show a density model of direction distribution; the mean magnetic susceptibility tensor represents sedimentary fabric tilted 14° northward with a weak tectonic overprint from N–S contraction or W–E extension; **B** – distribution in specimen coordinate system showing no preferable k1 direction related to sampling direction due to sampling forces; **C** – distribution in bedding coordinate system showing indistinct perpendicularity of k1 axes to bedding dip direction
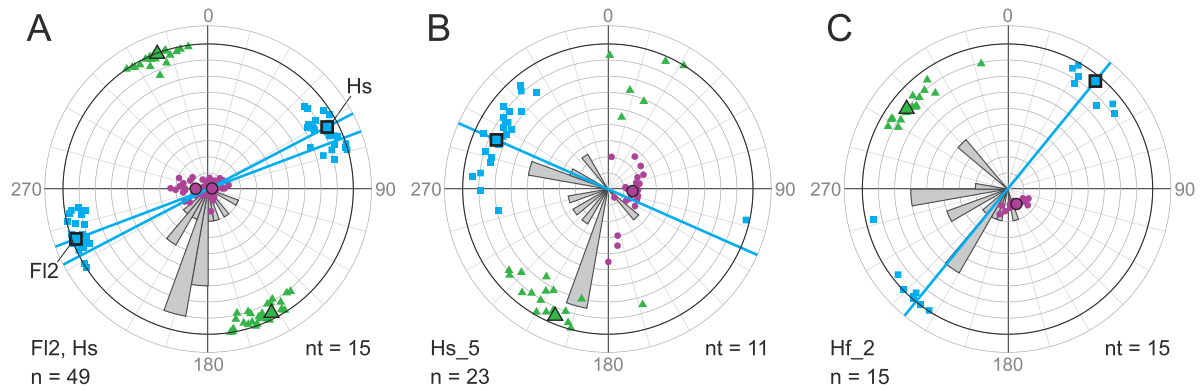
lar to bedding. Since the rocks are diversely tilted and axes k3 show variations from the mean direction, the question arises of how accurately the bedding orientation can be inferred from the k1–k2 plane (which is perpendicular to axis k3)? This may have a practical meaning in measuring bedding orientation within lithofacies having no lamination visible, which is common within massive siltstone lithofacies Fm. To test this, true bedding has been measured or extrapolated from neighbouring lithofacies. This makes a problem itself, because bedding is sometimes uneasy to measure and may have ±5° variations of dip angle and ±10° variations of dip direction within 10–20 cm of rock exposure. This diversity may be responsible for variations in k3 direction as well. The mean measured bedding orientation has been used as a local coordinate system – every specimen susceptibility ellipsoid has been rotated about a horizontal axis perpendicular to dip direction through a dipping angle. After this operation, all principal susceptibility axes are such as if the bedding was horizontal (Fig. 12).

The worse coincidence between ideal (vertical) axis and k3 is shown by lithofacies Gmm, due to the depositional mechanism discussed before. Lithofacies CL_1, Fm_4, Hs_5, and Hs_3 are not reliable, because of the sampling technique which included sampler turning to overcome rock friction and probably might have led to specimen rotation in the sampler. Other specimens collected precisely revealed good coincidence between the bedding and mean k1–k2 plane. The deviation between the ideal (vertical) and k3 axes ranged from 2.5 to 11.5°. Inaccuracy of sampling is estimated to be around ±5°, so improving sampling precision can probably reduce the deviation range further to a

few degrees. Additionally, the rock has observable bedding variations, which explain the gained range enough. Lithofacies comparison shows that the coincidence between the AMS k1–k2 plane and true bedding is independent of lithofacies type, which was surprising considering various degrees and shapes of anisotropy. Taking all above into account, interpreting the bedding orientation from the mean k1–k2 plane seems to be an acceptable method having accuracy at around 10°.

Directions of axes k1 can be interpreted as either sedimentary- or tectonic-determined. As mentioned before, the mean k1 direction of all specimens is W–E, which complies with the inferred N–S contraction that probably has led to northward tilting. However, a few lithofacies have k1 direction which does not fit this trend: CL_1, Hf_2, Fl2, Hs, Hs_3, Hs_5, and Fm_3 (Fig. 12). If a local stress direction differed from the main N–S trend, as shown by the variations in the bedding dip direction and angle (Fig. 2B), axis k1 would probably follow this local stress and remain perpendicular to the dip direction. This has been tested, however, k1 directions cannot be explained in this way. Another possibility is to look for a sedimentary factor which might have determined these directions. Four lithofacies: Hf_2, Fl2, Hs, and Hs_5 have been collected at exposures where ripple cross-lamination has been examined for palaeotransport directions (Łoziński et al., 2015). This means that a current was an important factor during deposition and might have led to a specific grain orientation and appropriate magnetic anisotropy. The comparison between axes k1 and the corresponding palaeotransport measurements is shown in Figure 13. Although some correspondence can be observed, transport directions are wide-range

Fig. 11. Different principal direction distributions (geographic coordinate system) determined by lithofacies type

A – lithofacies Gmm represents chaotic distribution of principal directions being a result of debris-flow deposition; **B** – lithofacies CL directly overlying lithofacies Gmm has dense distribution of k3 axes around its mean direction and sparse distribution of k1 and k2 axes; this is almost a perfect sedimentary AMS fabric, although some distinction between k1 and k2 is present; **C** – lithofacies Fm has well-defined dense distribution of axes directions around their means; note that some large susceptibility specimens (Km > 300 x 10^{-6} [SI], unfilled symbols) have their principal directions far from mean directions (sample Fm)

Fig. 12. Principal directions of mean tensors for all samples rotated according to a bedding coordinate system of corresponding sample

Closer the k3 axis (violet) to the midpoint of the graph, better the coincidence of rock bedding and k1–k2 plane of oblate ellipsoid (see text for interpretations); sample Gmm is poorly fitting this pattern due to its chaotic anisotropy resulted from the debris-flow sedimentation process; colours and symbols as in Figure 10

trending from S to NW, thus there is a huge chance that any axis would fit some transport direction. Moreover, a superposing of sedimentary and tectonic effect might have been involved. The other sedimentary feature – oblate grains imbrication may result in a k1–k2 plane tilting from the bedding plane (Tarling and Hrouda, 1993). However, this subtle feature probably cannot be determined due to weak measuring accuracy. A sedimentary explanation for unusual k1 directions seems to be the best so far, especially because it concerns lithofacies deposited under the influence of a weak current which favoured the formation of delicate sedimentary structures, and probably preferred grain orientation as well. However, we believe that data presented here is not sufficient to prove this.

DISCUSSION

FACTORS DETERMINING AMS

The comparison of bulk magnetic susceptibility with mineral composition obtained from X-ray diffraction (Fig. 9A) shows that this dependency is ambiguous. It was expected that magnetic susceptibility should provide a useful tool to determine the clay minerals to quartz ratio, but this two-component model is generally not satisfying for investigated multi-mineral deposits. However, this model could be applied to homogeneous deposits such as offshore-lake clayey and silty lithofacies CL, Fl, and Hs. Also, the bulk magnetic susceptibility Km is still useful for determining the presence of some high-susceptibility components, probably iron compounds, which represent different contents depending on lithofacies type.

The magnetic susceptibility and its anisotropy analysis always raises the question of which geological factors determine the acquired AMS fabric. While the bulk magnetic susceptibility reflects general specimen mineral composition, the anisotropy fabric is believed to be dependent on mineral composition, as well as sedimentary environment and tectonic deformation (see Hrouda, 1982 and references therein). The anisotropy of magnetic susceptibility can be also altered by the sampling process, especially when sediment is fresh and weakly consolidated (e.g., Copons et al., 1997; Shimono et al., 2014). When the hammered sampler is used, the largest sampling force appears in the direction of sampling, and the corresponding reorientation of k1 and k2 axes may occur. This can be verified by comparison of results obtained in different sampling directions, as performed within this study. However, no such correlation is observed showing that the deposits have been sufficiently consolidated before. The obtained AMS fabric represents predominantly oblate anisotropy with k3 axes perpendicular to bedding and k1 and k2 axes concentrated in the W–E and N–S directions (respectively, Fig. 10A) regardless of sampling direction.

The ellipsoid axes directions have been widely used to analyse weak deformations in sedimentary basins (e.g., Graham, 1966; Winkler et al., 1997; Parés et al., 1999; Kanamatsu et al., 2001; Kawamura and Ogawa, 2004). According to the methodology used, the k1 and k2 axes concentration near the W–E and N–S directions within studied specimens suggests that the orig-

**Fig. 13. Comparison of palaeotransport directions (grey bars; Łoziński et al., 2015)
with k1 directions of corresponding samples**

The coincidence of those two may be related to the orientation of elongated grains, determined by a current during sedimentation; the number of AMS specimens is n, and the number of transport direction measurements is nt; the mean k1 direction almost fits transport directions within sample Fl2 and Hs (A), and quite well within samples Hs_5 (B) and Hf_2 (C); however, the diversity of transport directions is high, so there is a chance of random fitting; blue squares and lines, large square = mean value; rotated – see Figure 12

inal sedimentary AMS fabrics has been weakly overprinted by tectonic deformation. A sedimentary factor being a result of current-driven grain orientation can be present as well, however, the tectonic factor is confirmed by the fact that axes grouping occurs within all samples representing different sedimentary regimes including suspension-fallout sedimentation. The sedimentary factor might have led to deviation of k1 and k2 axes from the common W–E and N–S directions, but the wide range of transport directions and obtained measuring accuracy make the importance of this factor ambiguous.

Tectonically induced AMS fabric with k1 oriented in the W–E direction implies the largest tectonic compression in the N–S direction. However, the AMS fabric itself does not determine the tectonic regime; N–S contraction, W–E extension or oblique strike-slip movements are possible. The general compression close to the N–S direction is accepted by most authors using different approaches, e.g. fractured clasts studies (NE to NNE compression; Tokarski and Zuchiewicz, 1998), geophysical surveys (NNE compression; Pomianowski, 2003), and detailed structural investigations (NNW compression near the Oravica outcrop; Struska, 2008). It coincides also with the northward bedding inclination in the Oravica section as a result of N–S contraction (k1 axes being mostly perpendicular to the bedding dip direction; Fig. 10C). However, normal faults existing in the Oravica section (Łoziński et al., 2015) and the general W–E basin extension suggested by Peškova et al. (2009) can support the extensional AMS fabric origin as well. Nevertheless, the maximal tectonic compression in the N–S direction seems to be well-confirmed.

AMS FACIES

Studied samples have revealed a wide variety of AMS features showing that the AMS method may offer a tool for recognizing sedimentary aspects of investigated deposits. However, a set of at least 20 specimens from one lithofacies is advisable to ensure a good statistic sample. A set of unique AMS features characteristic for each lithofacies within the Oravica section is introduced in Table 2. The very good estimation of sedimentary environment can be obtained for a lacustrine setting, where all discussed parameters: Km, P, and T are coherent (Fig. 4). More-

over, Km and T parameters decrease upward the lake sequence, which probably reflects increment of deposition of quartz-bearing silts during lake filling. Both bulk susceptibility Km and degree of anisotropy P of initial (CL) and terminal (Hs_5) lake deposits are varied, showing that coherent susceptibility parameters may be found only within offshore long-lasting lake settings where grain sorting is strongest. The opposite characteristics are represented by debris-flow lithofacies Gmm, having a wide variety of those parameters and the unique chaotic distribution of principal directions (Fig. 11A). Thus, the AMS method reveals a great potential in recognizing the internal structure of the conglomerate and breccia matrix, and may allow distinguishing between debris-flow and river/alluvial fan deposits.

The floodplain lithofacies Fm can be recognized easily with the low degree of anisotropy P and the shape parameter T being low or negative (Fig. 4). The presence of negative T values (lineation is greater than foliation) within one lithofacies type (samples Fm, Fm_3, Fm_4) is probably a result of weak tectonic overprint within deposits that originally gained even weaker sedimentary oblate fabric due to root bioturbation and a chaotic process of floodplain deposition. This example shows that negative T values may appear as a result of interplay between sedimentary and tectonic factors, especially if a general degree of anisotropy is low.

The ephemeral lake (e.g., oxbow lake, marsh) lithofacies Cl2 and the swamp lithofacies CCL have considerably high anisotropy P and shape T parameters, but not coherent. This can be explained by instability of terrestrial environment: floods bringing detrital material, changing water level and plant vegetation, as well as formation of iron compounds in geochemical/microbial processes within a palaeosol, resulting in a high susceptibility of some specimens. Sample CL is similar to sample CL2 and was probably influenced by the same processes at the initial stage of the long-lasting lake. The clay minerals and plant detritus compound is the most anisotropic sediment, as observed within coaly claystone CCL. The river lithofacies St has coherent P and T parameters being similar to lake deposits, but it has lower anisotropy P (1.1–1.3) and incoherent susceptibility Km (Fig. 4). Similarly, the heterolithic lithofacies Hs has various values of Km and P, probably due to the variable quartz/clay minerals ratio. However, these two lithofacies are not well-constrained in AMS measurements.

Unique AMS features within the Oravica section allowing lithofacies and sedimentary environment estimation

Lithofacies (environment)	Samples	Unique AMS features of studied samples (AMS facies)	Quality of lithofacies estimation
CCL (swamp)	CCL	Km: low (100–200 x 10^{-6} [SI]) P: high (1.06–1.12) T: high (0.5–1.0)	average
CL (lake with terrestrial influence)	CL, CL2	Km: incoherent P: incoherent T: high (0.0–1.0)	average
Fm (floodplain)	Fm, Fm_3, Fm_4	20–30% of specimens are prolate (T <0) P: low (1.00–1.04) T: various (−0.7 to 0.8)	good
St (river)	St	–	poor
Hs (lake-nearshore)	Hs_5	–	poor
Hs (lake-offshore)	Hs, Hs_3	Km, P, and T: coherent Km: average (120–405 x 10^{-6} [SI]) P: average (1.02–1.05) T: high (0.5–1.0)	good for determining lacustrine setting
Hf (lake-offshore)	Hf_2		
Fl (lake-offshore)	Fl, Fl2		
CL (lake-offshore)	CL_1		
Gmm (colluvium)	Gmm	chaotic k3 directions	good

Since the presented key for lithofacies recognition is conceptual and has been created for the Oravica outcrop only, it should be pointed out here that the AMS features in other outcrops may vary. However, the AMS fabric has been proved to be responsive to many subtle phenomena including: suspension fallout/current deposition, fluctuations of quartz-clay minerals, organic matter admixtures, bioturbation, and Fe redistribution in diagenetic processes. The AMS method has a great practical potential in recognizing sedimentary features and bedding orientation of deposits, especially when they are not visible macroscopically or the studied outcrop is small. Since the massive structure of deposits is very common in the Orava-Nowy Targ Basin, the AMS analysis may provide a considerable support for the basin study.

CONCLUSIONS

– Mineral composition of studied deposits is multicomponent, thus the correlation between mineral content and bulk susceptibility Km is ambiguous. However, samples with a narrow susceptibility range provide parameter Km as a rough indicator for the clay mineral to quartz ratio. This tool may be applied to analyse offshore lacustrine deposits.

– AMS ellipsoid directions have been determined mainly by weak tectonic deformation with the highest tectonic compression being N–S.

– Bulk magnetic susceptibility, anisotropy degree and anisotropy shape are strongly determined by the lithofacies type.

– Five AMS facies distinguished here allow recognizing the following sedimentary settings: debris-flow deposition, offshore lake, nearshore/ephemeral lake, floodplain, and swamp.

– Sedimentological transport impact on the AMS directions is ambiguous due to the method accuracy and tectonic overprint.

– Mean k1–k2 plane orientation can be used as a bedding estimation with 10° error. This may be useful especially when analysing apparently massive sediments.

– Similar contents and X-ray traces of clay minerals within basement colluvium and overlying sediments suggest that studied deposits have been derived from one source area, the Podhale Synclinorium.

REFERENCES

Baumgart-Kotarba, M., 1996. On origin and age of the Orava Basin, West Carpathians. Studia Geomorphologica Carpatho--Balcanica, **30**: 101–116.

Baumgart-Kotarba, M., 2001. Continuous tectonic evolution of the Orava basin from Late Badenian to the present-day. Geologica Carpathica, **52**: 103–110.

Bojanowski, M., Jaroszewicz, E., Košir, A., Łoziński, M., Marynowski, L., Wysocka, A., Derkowski, A., 2016. Root-related rhodochrosite and concretionary siderite formation in oxygen-deficient conditions induced by a ground-water table rise. Sedimentology, **63**: 523–551.

Callaway, W.S., McAtee, J.L., 1985. Magnetic susceptibilities of representative smectites. American Mineralogist, **70**: 996–1003.

Chadima, M., Jelínek, V., 2009. Anisoft 4.2: anisotropy data browser for Windows. AGICO, Brno, Czech Republic, http://www.agico.com

Chung, F.H., 1974a. Quantitative interpretation of X-ray diffraction patterns of mixtures. I. Matrix-flushing method for quantitative multicomponent analysis. Journal of Applied Crystallography, **7**: 519–525.

Chung, F.H., 1974b. Quantitative interpretation of X-ray diffraction patterns of mixtures. II. Adiabatic principle of X-ray diffraction analysis of mixtures. Journal of Applied Crystallography, **7**: 526–531.

Copons, R., Parés, J.M., Dinarès-Turell, J., Bordonau, J., 1997. Sampling induced AMS in soft sediments: a case study in holocene glaciolacustrine rhythmites from Lake Barrancs (Central Pyrenees, Spain). Physics and Chemistry of the Earth, **22**: 137–141.

Garecka, M., 2005. Calcareous nannoplankton from the Podhale Flysch (Oligocene-Miocene, Inner Carpathians, Poland). Studia Geologica Polonica, **124**: 353–370.

Graham, J.W., 1954. Magnetic susceptibility anisotropy, an unexploited petrofabric element. GSA Bulletin, **65**: 1257–1258.

Graham, J.W., 1966. Significance of magnetic anisotropy in Appalachian sedimentary rocks. Geophysical Monograph Series, **10**: 627–648.

Gross, P., Köhler, E., Haško, J., Halouzka, R., Mello, J., Nagy, A., 1993. Geológia južnej a východnej Oravy (in Slovak) (Geology of southern and eastern Orava). Štátny Geologický Ústav Dionýza Štúra. Bratislava.

Hrouda, F., 1982. Magnetic anisotropy of rocks and its application in geology and geophysics. Geofyzika, Brno: 37–82.

Hunt, C.P., Moskowitz, B.M., Banerjee, S.K., 1995. Magnetic properties of rocks and minerals. In: Rock Physics and Phase Relations: a Handbook of Physical Constants (ed. T.J. Ahrens). AGU Reference Shelf, **3**: 189–204.

Ising, G., 1942. On the magnetic properties of varved clay. Arkiv för Matematik, Astronomi och Fysik, **29a**: 1–37.

Jaroszewicz, E., Grafka, O., Marynowski, L., 2013. Source-indicating and maturity-related biomarkers from Miocene deposits from Orava–Nowy Targ basin – preliminary results. 30th Annual Meeting of the TSOP 2013, Sosnowiec, Poland: 56.

Jelínek, V., 1977. The statistical theory of measuring anisotropy of magnetic susceptibility of rocks and its application. Geofyzika, Brno: 1–88.

Jelínek, V., 1978. Statistical processing of anisotropy of magnetic susceptibility measured on groups of specimens. Studia Geophysica et Geodaetica, **22**: 50–62.

Kanamatsu, T., Herrero-Bervera, E., Taira, A., 2001. Magnetic fabrics of soft-sediment folded strata within a neogene accretionary complex, the Miura group, central Japan. Earth and Planetary Science Letters, **187**: 333–343.

Kawamura, K., Ogawa, Y., 2004. Progressive change of pelagic clay microstructure during burial process: examples from piston cores and ODP cores. Marine Geology, **207**: 131–144.

Kołcon, I., Wagner, M., 1991. Brown coal from Neogene sediments of the Orawa-Nowy Targ basin – petrological study (in Polish with English summary). Geological Quarterly, **35** (3): 305–322.

Lexa, J., Bezák, V., Elečko, M., Mello, J., Polák, M., Potfaj, M., Vozár, J., 2000. Geological Map of the Western Carpathians and Adjacent Areas, 1:500 000. Geological Survey of Slovak Republic, Bratislava.

Łoziński, M., Wysocka, A., Ludwiniak, M., 2015. Neogene terrestrial sedimentary environments of the Orava-Nowy Targ Basin: a case study of the Oravica River section near Čimhová, Slovakia. Geological Quarterly, **59** (1): 21–34.

Martín-Hernández, F., Hirt, A.M., 2003. The anisotropy of magnetic susceptibility in biotite, muscovite and chlorite single crystals. Tectonophysics, **367**: 13–28.

Mazzoli, S., Szaniawski, R., Mittiga, F., Ascione, A., Capalbo, A., 2012. Tectonic evolution of Pliocene–Pleistocene wedge-top basins of the southern Apennines: new constraints from magnetic fabric analysis. Canadian Journal of Earth Sciences, **49**: 492–509.

Nagy, A., Vass, D., Petrík, F., Pereszlényi, M., 1996. Tectogenesis of the Orava Depression in the light of latest biostratigraphic investigations and organic matter alteration studies. Slovak Geological Magazine, **1/96**: 49–58.

Olszewska, B., Wieczorek, J., 1998. The Paleogene of the Podhale Basin (Polish Inner Carpathians) – micropaleontological perspective (in Polish with English summary). Przegląd Geologiczny, **46**: 721–728.

Parés, J.M., 2015. Sixty years of anisotropy of magnetic susceptibility in deformed sedimentary rocks. Frontiers in Earth Science, **3**: 1–12.

Parés, J.M., van der Pluijm, B.A., Dinarès-Turell, J., 1999. Evolution of magnetic fabrics during incipient deformation of mudrocks (Pyrenees, northern Spain). Tectonophysics, **307**: 1–14.

Pešková, I., Vojtko, R., Starek, D., Sliva, L., 2009. Late Eocene to Quaternary deformation and stress field evolution of the Orava region (Western Carpathians). Acta Geologica Polonica, **59**: 73–91.

Pomianowski, P., 2003. Tectonics of the Orava-Nowy Targ Basin – results of the combined analysis of the gravity and geoelectrical data (in Polish with English summary). Przegląd Geologiczny, **51**: 498–506.

R Core Team, 2015. R: A Language and Environment for Statistical Computing. R Foundation for Statistical Computing. Vienna, Austria. https://www.r-project.org

RStudio Team, 2015. RStudio: Integrated Development for R. RStudio, Inc., Boston, MA. http://www.rstudio.com

Shimono, T., Yamazaki, T., Inoue, S., 2014. Influence of sampling on magnetic susceptibility anisotropy of soft sediments: comparison between gravity and piston cores. Earth, Planets and Space, **66** (3).

Sikora, W., Wieser, T., 1974. Utwory piroklastyczne w utworach neogeńskich śródgórskiej niecki Orawy-Nowego Targu (in Polish). Kwartalnik Geologiczny, **18** (2): 441–443.

Soták, J., 1998a. Sequence stratigraphy approach to the Central Carpathian Paleogene (Eastern Slovakia): eustasy and tectonics as controls of deep sea fan deposition. Slovak Geological Magazine, **4**: 185–190.

Soták, J., 1998b. Central Carpathian Paleogene and its constraints. Slovak Geological Magazine, **4**: 203–211.

Struska, M., 2008. Neogeńsko-czwartorzędowy rozwój strukturalny Kotliny Orawskiej w świetle badań geologicznych, geomorfologicznych oraz teledetekcyjnych (in Polish). Ph.D thesis, Wydział Geologii, Geofizyki i Ochrony Środowiska, AGH, Kraków.

Tarling, D.H., Hrouda, F., 1993. The Magnetic Anisotropy of Rocks. Chapman and Hall, London.

Tokarski, A.K., Zuchiewicz, W., 1998. Fractured clasts in the Domański Wierch series: Contribution to structural evolution of the Orava Basin (Carpathians, Poland) during Neogene through Quaternary times (in Polish with English summary). Przegląd Geologiczny, **46**: 62–66.

Tokarski, A.K., Świerczewska, A., Zuchiewicz, W., Starek, D., Fodor, L., 2012. Quaternary exhumation of the Carpathians: a record from the Orava-Nowy Targ Intramontane Basin, Western Carpathians (Poland and Slovakia). Geologica Carpathica, **63**: 257–266.

Watycha, L., 1976. The Neogene of the Orava-Nowy Targ Basin (in Polish with English summary). Geological Quarterly, **20** (3): 575–585.

Wickham, H., 2009. ggplot2: Elegant Graphics for Data Analysis. Springer, New York.

Wiewióra, A., Wyrwicki, R., 1980. Clay minerals of the Neogene sediments in the Orava-Nowy Targ basin (in Polish with English summary). Geological Quarterly, **24** (2): 333–348.

Winkler, A., Alfonsi, L., Florindo, F., Sagnotti, L., Speranza, F., 1997. The magnetic anisotropy of rocks: principles, techniques and geodynamic applications in the Italian peninsula. Annals of Geophysics, **40**: 729–740.

Ziółkowski, P., Hinnov, L.A., 2010. High-resolution cyclostratigraphic analysis of the magnetic susceptibility record from the Upper Bajocian to Upper Bathonian of Central Poland and the mineralogical link between magnetic susceptibility and palaeoclimatic changes. Earth Science Frontiers, **17**: 37.